High efficiency hexagonal boron nitride neutron detectors with 1 cm² detection areas

A. Maity, [iD] S. J. Grenadier, [iD] J. Li, [iD] J. Y. Lin, [iD] and H. X. Jiang[a) [iD]

AFFILIATIONS

Department of Electrical and Computer Engineering, Texas Tech University, Lubbock, Texas 79409, USA

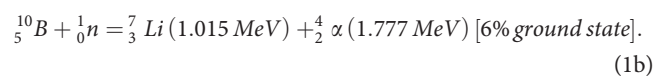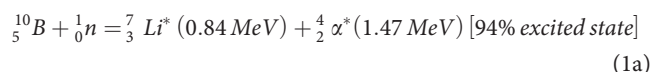[a)]Author to whom correspondence should be addressed: hx.jiang@ttu.edu

ABSTRACT

We report the realization of 1 cm² hexagonal boron nitride (h-BN) thermal neutron detectors with an unprecedented detection efficiency of 59%. This was achieved through improvements in material quality, as reflected in a sixfold enhancement in the electron mobility and lifetime product and a threefold reduction in the surface recombination field, which resulted in a higher detection efficiency at a lower applied electric field over that of a previous state-of-the-art lateral detector with a detection area of 30 mm². The attainment of 1 cm² h-BN neutron detectors capable of retaining a high detection efficiency represents a significant milestone toward the practical applications of h-BN detectors.

Published under license by AIP Publishing. https://doi.org/10.1063/1.5143808

Geothermal and well-logging industries employ tools that use neutron detectors to determine the formation properties of rocks, including water content and porosity.[1] From a national security perspective, neutron detectors are indispensable for detecting the signatures of special nuclear materials and sensing any illicit movement of fissile materials at the ports of entry.[2] Pressurized Helium-3 (^{3}He) gas-filled detectors are widely deployed as an industry standard.[3] Despite having a very high thermal neutron capture cross section of $\sim$5330 barns, the intrinsic low atomic density of these gas-filled detectors translates to long absorption lengths for thermal neutrons, thereby making them inherently bulky. The requirement of high pressurization also limits their uses at temperatures of $<175\,^\circ$C, whereas the required operating temperatures for deep well and geothermal logging may exceed 300 $^\circ$C. Other shortcomings of ^{3}He detectors include the requirement of high biasing voltages (>1000 V), slow response speed ($\sim$ms), high cost, and limited availability. Therefore, solid-state neutron detectors with high sensitivities with the potential to replace Helium-3 gas-filled neutron detectors are a highly sought-after technology.

Being a wide bandgap semiconductor ($E_g > 6.0$ eV), h-BN is not only well known for its deep UV photonic device applications, but has also emerged as a highly efficient material for the fabrication of solid-state neutron detectors,[4–12] in which the detection of neutrons is based on the following nuclear reaction between neutrons and boron-10 (^{10}B) atoms:[3]

$$^{10}_{5}B + ^{1}_{0}n = ^{7}_{3}Li^* \left(0.84\,MeV\right) + ^{4}_{2}\alpha^* \left(1.47\,MeV\right) \left[94\%\,excited\,state\right]$$
(1a)

$$^{10}_{5}B + ^{1}_{0}n = ^{7}_{3}Li \left(1.015\,MeV\right) + ^{4}_{2}\alpha \left(1.777\,MeV\right) \left[6\%\,ground\,state\right].$$
(1b)

Due to the large thermal neutron absorption cross section of the ^{10}B isotope ($\sigma \sim 3840$ barns $= 3.84 \times 10^{-21}$ cm²) and the high atomic density of ^{10}B ($\sim 5.5 \times 10^{22}$/cm³) in 100% ^{10}B-enriched h-BN (h-^{10}BN), the thermal neutron absorption length (λ) in h-^{10}BN is as short as $\sim$47.3 μm [$\lambda = \alpha^{-1} = (N\sigma)^{-1} = (5.5 \times 10^{22} \times 3.84 \times 10^{-21})^{-1}$ cm].[7] Therefore, h-^{10}BN neutron detectors are inherently lightweight and compact with excellent form factors. The high electrical resistivity ($>10^{12}$ Ω·cm) and high temperature stability of h-BN make these detectors suitable for high temperature operation. Furthermore, h-^{10}BN neutron detectors require a lower operating voltage than ^{3}He gas detectors because h-^{10}BN is a semiconductor and have a demonstrated low sensitivity to gamma radiation due to the low atomic numbers of constituent B and N atoms.[7]

Due to the nature of low neutron flux from a primitive nuclear device ($\sim 3 \times 10^5$ neutrons/s) and low reflectance of neutrons in porosity measurements, large size detectors capable of providing high sensitivities are desirable for practical uses. The sensitivity of a detector or the count rate (C_R) detected by a detector is proportional to its detection efficiency (η) and detection area (A_d), i.e., $C_R = \varphi \eta A_d$, where φ is the neutron flux. However, there are technical challenges to scale up the detector size, which include increased dark current, capacitance, and surface recombination field (E_s), all of which tend to decrease the detection efficiency. It was shown recently that compared

to vertical detectors consisting of planar contacts on top and bottom, the adoption of a lateral detector configuration can alleviate these issues to some extent, which led to the demonstration of h-^{10}BN detectors with a detection area of 0.3 cm^2 and a detection efficiency of ∼50%.[12] In this work, we report the realization of 1 cm^2 h-BN thermal neutron detectors with an unprecedented detection efficiency of 59%. Improved material quality plays a key role in enabling the scale up to this detection area, as reflected in the increased charge carrier mobility-lifetime ($\mu\tau$) product and reduced surface recombination field (E$_s$), which are two important parameters greatly influencing the charge collection efficiency and hence the overall detection efficiency of h-^{10}BN neutron detectors.[10–12]

Epilayers of h-^{10}BN of ∼100 μm in thickness were deposited on c-plane sapphire substrates of 4-in. in diameter, using metal-organic chemical vapor deposition (MOCVD). Based on the insights of previous studies,[9–13] a low temperature BN buffer layer of about 20 nm in thickness was deposited on the c-plane sapphire substrate at about 800 °C prior to the growth of the h-^{10}BN epilayer, whereas the growth temperature of the subsequent thick h-^{10}BN epilayer was ∼1400 °C. The primary purpose of using a reduced growth temperature of 1400 °C in the present work as compared to that of > 1400 °C in previous studies[10–12] was to reduce the oxygen diffusion from the sapphire substrate,[13] whereas oxygen impurities in h-BN are known to occupy nitrogen sites (O$_N$) acting as donors.[14] Moreover, the presence of O$_N$ donor impurities tends to decrease the formation energies of boron vacancy (V$_B$) related deep level defects in h-BN,[14] which are expected to be detrimental to the charge collection efficiency of h-BN detectors. Layer structured h-BN has a different thermal expansion coefficient than the sapphire substrate, enabling natural separation of thick h-^{10}BN layers from sapphire substrates during cooling down after epi-growth. An optical image of a portion of the diced h-^{10}BN wafer used in this study is shown in Fig. 1(a). This freestanding h-^{10}BN wafer was diced into strips of ∼1.3 mm in width. Adopting the same and proven lateral device architecture used in the 0.3 cm^2 detector,[12] we combined 5 strips with lengths varying from 13.5 to 17 mm to form a detector with a total detection area of 1 cm^2. A highly resistive adhesive material was used to mount these strips on a sub-mount (sapphire). E-beam evaporation was used to deposit a metal bi-layer of Ni (100 nm) and Au (40 nm) on the clipped edges of the h-^{10}BN strips using a shadow mask of 1.1 mm width leaving around ∼100 μm metal covering on the edges, as schematically depicted in Fig. 1(b). The finished 1 cm^2 h-^{10}BN detector is shown in Fig. 1(c).

The dark current–voltage (I–V) measurements were performed for the 1 cm^2 detector from 0 to 500 V and the result is shown in Fig. 2(a). A linear fit of the I–V characteristic provides values of resistance, R = 1.77 × 10^{12} Ω and resistivity, ρ = 1.05 × 10^{12} Ω·cm. A deuterium UV lamp (DS421, Acton Research Corporation, spectral range of 190–350 nm) was used as an excitation light source for characterizing the I–V characteristics under illumination. A metal mask was used to allow UV light to enter and illuminate the h-^{10}BN strips only near one electrode, as illustrated in Fig. 1(b). If the electrode near the illuminated area is negatively (positively) biased, electrons (holes) must travel a longer distance than holes (electrons) before being collected at the electrodes, enabling photocurrent measurements for electrons and holes separately. It was found that the photocurrent due to hole transport is extremely low in comparison to that of electron transport, which indicates that the h-^{10}BN epilayer has a higher
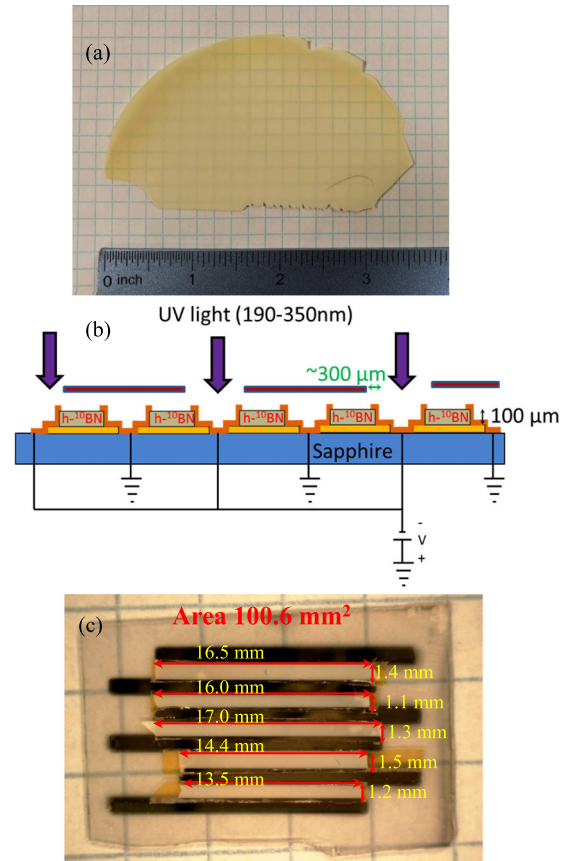
FIG. 1. (a) Optical image of a portion of the diced h-^{10}BN sample used in this work. (b) Schematic diagram of detector strips mounted on a sapphire sub-mount with UV light illuminated through a metal mask, allowing the measurement of electron and hole transport separately. (c) Optical image of a 1 cm^2 neutron detector fabricated from a 100 μm thick h-^{10}BN freestanding wafer by combining five detector strips.

concentration of donors than acceptors. The results again indicate that the background carrier concentration and hence the dark current are contributed by electrons from O$_N$ donors due to the unavoidable oxygen diffusion from the sapphire substrate to the h-^{10}BN film during MOCVD growth.[10,13]

The measured I–V characteristics of electron transport under UV illumination are shown in Fig. 2(b). To determine the charge carrier $\mu\tau$ product and surface recombination field E$_s$ = s/μ, the measured photocurrent in Fig. 2(b) was fitted by Many's equation,[15]

$$I_i(V) = I_{0,i}\eta_{c,i} = I_{0,i}\left[\frac{V_b\mu_i\tau_i\left(1 - e^{-\frac{W^2}{V_b\mu_i\tau_i}}\right)}{W^2\left(1 + \frac{s_iW}{\mu_iV_b}\right)}\right] \quad (i = e, h). \quad (2)$$

Here, the saturation current is denoted as I$_0$, and $\mu_h\tau_h$ ($\mu_e\tau_e$) and s$_h$ (s$_e$) are the mobility-lifetime product and surface recombination velocity for holes (electrons), respectively. V$_b$ is the applied voltage between two electrodes of distance W, providing an applied electric field of $E_a = \frac{V_b}{W}$. The numerator and the denominator term of Eq. (2) describe the charge collection efficiency limited by the bulk trapping effect (or
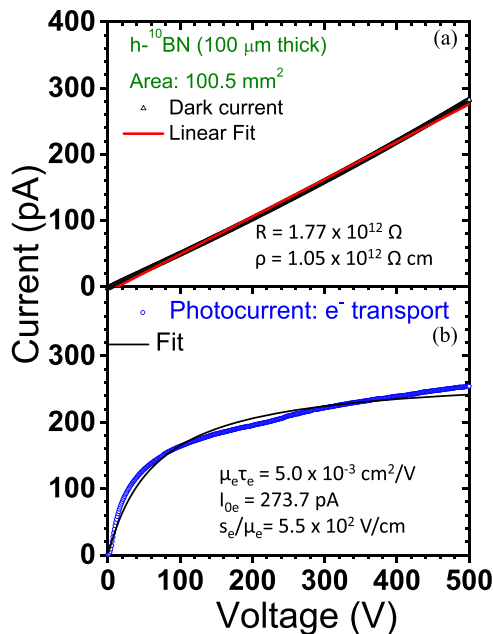
FIG. 2. Current–voltage characteristics measured for the device configuration shown in Fig. 1(b): (a) in the dark and (b) under UV radiation for electron transport.

FIG. 3. Pulse height spectra of the 1 cm^2 h-^{10}BN detector. The red curve is the response to thermal neutrons which was recorded by placing the detector 1 m away from the ^{252}Cf source moderated by a HDPE cube. The blue curve is the background (or dark) counts measured at the same bias voltage. The green curve is the response to gamma photons emitted from a ^{137}Cs source measured at the same bias voltage.

$\mu\tau$ product) and "surface recombination field" or the ratio of surface recombination velocity to mobility ($E_s = s/\mu$), respectively,[9–11] whereas both $\mu\tau$ and s/μ are directly correlated with the overall material quality. From Eq. (2), conditions for a high charge collection efficiency are (a) $\frac{W^2}{V_b\mu_i\tau_i} = \frac{W}{E_a\mu_i\tau_i} \ll 1$, which means that the charge carrier drift length ($E_a\mu_i\tau_i$) must be greater than the transit length (spacing between the electrodes, W) and (b) $\frac{s_i/\mu_i}{V_b/W} = \frac{E_s^i}{E_a} \ll 1$ (where $i = e, h$), which means that the applied electric field must be greater than the surface recombination field.[9–11] The measured values of $\mu_e\tau_e$ and s_e/μ_e for this detector were 5.0×10^{-3} cm^2/V and 5.5×10^2 V/cm, respectively, which provide values of $\frac{W^2}{V_b\mu_e\tau_e} \approx 0.007$ and $\frac{s_e/\mu_e}{V_b/W} \approx 0.14$ at a bias voltage of 500 V, and a theoretical charge collection efficiency of 87.4% under UV irradiation. It is important to recognize that the measured $\mu_e\tau_e$ product of this detector has been enhanced by a factor of 6, while E_s^e has been reduced by a factor of 3 in comparison to those of a previous reported state-of-the-art 0.3 cm^2 h-^{10}BN lateral detector.[12] These improvements were achieved primarily through MOCVD epitaxial growth optimization discussed above.

Figure 3 shows the pulse height spectra of this 1 cm^2 h-^{10}BN detector. The detector was placed 1 m away from a ^{252}Cf source with a radioactivity of 0.45 mCi ($\sim$1.95 $\times$ 10^6 n/s), moderated by a high-density polyethylene (HDPE) of 2.5 cm thickness.[5–12] The detection electronics were described in detail in a previous work.[10] The dark spectrum (blue) was recorded in the absence of any radiation source at 500 V, while the spectrum (red) under thermal neutron irradiation was measured at the same bias voltage. The green curve is the response to gamma photons emitted from a ^{137}Cs source under 10 mR/h exposure measured at the same bias voltage, which shows that the h-^{10}BN detector has a negligible response to gamma photons. The pulse height
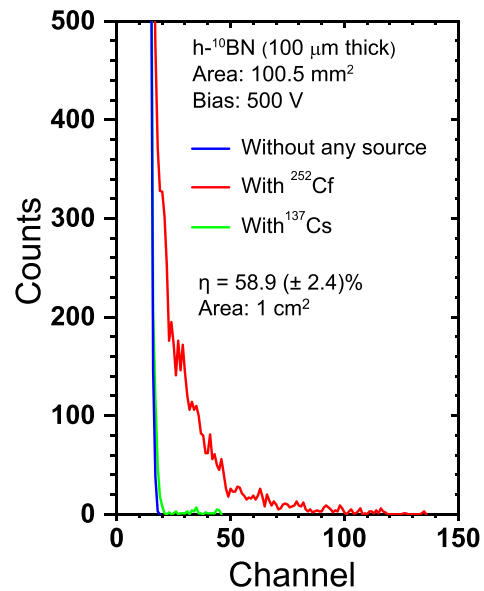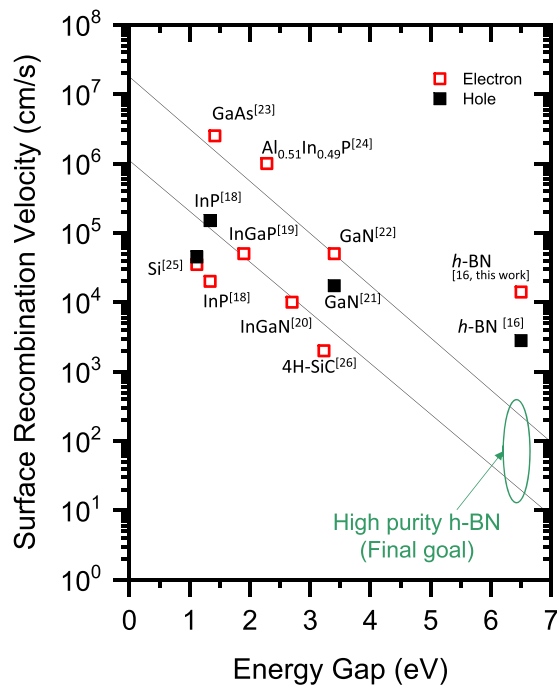
spectrum under thermal neutron radiation was integrated beyond the highest dark channel (low level discriminator) to obtain the total number of counts. By comparing the total number of counts detected by the h-^{10}BN detector to that of a commercial ^{6}LiF filled 4 cm^2 micro-structured semiconductor neutron detector (MSND Domino^{TM} V4) constructed from a combination of four 1 cm^2 detectors with a certified detection efficiency of 30 ($\pm$1)%, the detection efficiency (η) of our 1 cm^2 h-^{10}BN detector was determined to be 58.9 ($\pm$ 2.4) % at a bias voltage of 500 V, which represents the highest detection efficiency reported among all solid-state neutron detectors. We believe that improvements in the overall h-^{10}BN material quality, as reflected through the enhanced $\mu\tau$ product and reduced surface recombination field stand to enable the scale up of the detector size to 1 cm^2 while retaining a high detection efficiency of $\sim$59%. It is worth pointing out that as the material quality of thick h-^{10}BN epilayers further improves, h-^{10}BN detectors are expected to resolve the nuclear reaction sum peaks at 2.31 MeV and 2.792 MeV of Eq. (1), as demonstrated in low efficiency detectors fabricated from a very thin (2.7 μm) h-^{10}BN film.[6]

The performances of semiconductor devices, especially radiation detectors, are profoundly influenced by charge recombination at the surfaces and hence the surface recombination field and velocity are two very important figure of merits. The measured value of $s_e/\mu_e = 5.5 \times 10^2$ V/cm from Fig. 3 together with a recently measured electron mobility in the lateral direction in h-^{10}BN of $\mu_e = 35$ cm^2/V·s[16] allows us to deduce a value for the surface recombination velocity for electrons in h-^{10}BN of $s_e = 5.5 \times 10^2 \times 35 = 1.9 \times 10^4$ cm/s, which agrees well with a previous measured value of 1.4×10^4 cm/s.[16] To gain a better understanding of the relationship between surface recombination

velocities among various III–V semiconductors, we summarize in Fig. 4 surface recombination velocities of various materials, based on prior published data.[17–26] An interesting trend emerges from the combined data shown in Fig. 4, as previously noted,[17] is that the surface recombination velocity generally decreases with an increase in the bandgap. As h-BN has a bandgap of greater than 6 eV, the trend exhibited in Fig. 4 projects a value of s for h-BN to be $\sim 10^2$ cm/s. It is important to note that no surface treatment was employed in the processes of fabricating 1 cm^2 h-^{10}BN detectors reported here. Hence, the trend shown in Fig. 4 suggests that there is still significant room for improvement in the overall material quality and surface treatment processes for h-BN materials and devices. The emergence of h-^{10}BN for thermal neutron detectors as well as single crystal diamond and SiC for fast neutron detectors[27–29] opens up the potential to fulfill the shortcomings of ^{3}He gas detectors.

In summary, we have fabricated 1 cm^2 h-^{10}BN neutron detectors from a 100 μm thick freestanding h-^{10}BN epilayer with an unprecedented high detection efficiency of $\sim$59%. This realization was made possible through the improvements in the material quality as revealed by a sixfold enhancement in the $\mu\tau$-product and a 3 times reduction in E_s compared to those of a previous 0.3 cm^2 detector.[12] Without employing any surface treatment, the surface recombination velocity measured from this 1 cm^2 h-^{10}BN detector is $\sim$1.9 $\times$ 10^4 cm/s. The value obtained here combined with the data of surface recombination velocities reported from other III–V semiconductors suggested that the surface recombination velocity of h-BN can be as low as 10^2 cm/s with further improvements in material quality and device processing. The realization of 1 cm^2 h-BN neutron detectors capable of retaining a high detection efficiency represents a critical step toward the commercial adoption of high sensitivity h-^{10}BN neutron detectors for practical applications.

FIG. 4. Surface recombination velocities of representative semiconductors vs the energy bandgap E_g, with published data from Ref. 23 for GaAs, Ref. 18 for InP, Ref. 24 for Al$_{0.51}$In$_{0.49}$P, Ref. 20 for InGaN, Ref. 19 for InGaP, Refs. 21 and 22 for GaN, Ref. 25 for Si, Ref. 26 for 4H-SiC, and Ref. 16 for h-BN. The black lines serve as a guide to the eye revealing the trend of decreasing surface velocity with an increase in the energy bandgap of semiconductors.

REFERENCES

[1] J. Neal, L. Boatner, Z. Bell, H. Akkurt, and M. McCarthy, "Evaluation of neutron and gamma detectors for high-temperature well-logging applications," in Future of Instrumentation International Workshop (FIIW) (2011), pp. 172–175.

[2] W. A. Noonan, J. Hopkins Apl. Tech. Dig. **32**, 762 (2014).

[3] G. F. Knoll, Radiation Detection and Measurement, 4th ed. (John Wiley & Sons, 2010).

[4] J. Li, R. Dahal, S. Majety, J. Y. Lin, and H. X. Jiang, Nucl. Instrum. Methods Phys. Res., Sect. A **654**, 417 (2011).

[5] T. C. Doan, S. Majety, S. Grenadier, J. Li, J. Y. Lin, and H. X. Jiang, Nucl. Instrum. Methods Phys. Res., Sect. A **748**, 84 (2014); **783**, 121 (2015).

[6] T. C. Doan, J. Li, J. Y. Lin, and H. X. Jiang, AIP Adv. **6**, 075213 (2016).

[7] A. Maity, T. C. Doan, J. Li, J. Y. Lin, and H. X. Jiang, Appl. Phys. Lett. **109**, 072101 (2016).

[8] K. Ahmed, R. Dahal, A. Weltz, J. J. Q. Lu, Y. Danon, and I. B. Bhat, Appl. Phys. Lett. **110**, 023503 (2017).

[9] A. Maity, S. J. Grenadier, J. Li, J. Y. Lin, and H. X. Jiang, Appl. Phys. Lett. **111**, 033507 (2017).

[10] A. Maity, S. J. Grenadier, J. Li, J. Y. Lin, and H. X. Jiang, J. Appl. Phys. **123**, 044501 (2018).

[11] A. Maity, S. J. Grenadier, J. Li, J. Y. Lin, and H. X. Jiang, J. Appl. Phys. **125**, 104501 (2019).

[12] A. Maity, S. J. Grenadier, J. Li, J. Y. Lin, and H. X. Jiang, Appl. Phys. Lett. **114**, 222102 (2019).

[13] S. J. Grenadier, A. Maity, J. Li, J. Y. Lin, and H. X. Jiang, Appl. Phys. Lett. **112**, 162103 (2018).

[14] L. Weston, D. Wickramaratne, M. Mackoit, A. Alkauskas, and C. G. Van de Walle, Phys. Rev. B **97**, 214104 (2018).

[15] A. Many, J. Phys. Chem. Solids **26**, 575 (1965).

[16] S. J. Grenadier, A. Maity, J. Li, J. Y. Lin, and H. X. Jiang, Appl. Phys. Lett. **115**, 072108 (2019).

[17] K. A. Bulashevich and S. Y. Karpov, Phys. Status Solidi RRL **10**, 480 (2016).

[18] C. A. Hoffman, H. J. Gerritsen, and A. V. Nurmikko, J. Appl. Phys. **51**, 1603 (1980).

[19] S. J. Pearton, F. Ren, W. S. Hobson, C. R. Abernathy, and U. K. Chakrabarti, in Proceedings of the IEEE 6th International Conference on Indium Phosphide and Related Materials (IPRM) (1994), pp. 186–189.

[20] S. Zhang, Y. Li, S. Fathololoumi, H. P. T. Nguyen, Q. Wang, Z. Mi, Q. Li, and G. T. Wang, AIP Adv. **3**, 082103 (2013).

[21] J. Shakya, J. Y. Lin, and H. X. Jiang, Appl. Phys. Lett. **85**, 2104 (2004).

[22] R. Aleksiejūnas, M. Sūdžius, T. Malinauskas, J. Vaitkus, and K. Jarašiūnas, Appl. Phys. Lett. **83**, 1157 (2003).

[23] L. Jastrzebski, J. Lagowski, and H. C. Gatos, Appl. Phys. Lett. **27**, 537 (1975).

[24] M. Boroditsky, I. Gontijo, M. Jackson, R. Vrijen, E. Yablonovitch, T. Krauss, C.-C. Cheng, A. Scherer, R. Bhat, and M. Krames, J. Appl. Phys. **87**, 3497 (2000).

[25] D. Baek, S. Rouvimov, B. Kim, T.-C. Jo, and D. K. Schroder, Appl. Phys. Lett. **86**, 112110 (2005).

[26]Y. Mori, M. Kato, and M. Ichimura, J. Phys. D: Appl. Phys. **47**, 335102 (2014).

[27]C. Cazzaniga, E. A. Sundén, F. Binda, G. Croci, G. Ericsson, L. Giacomelli, G. Gorini, E. Griesmayer, G. Grosso, G. Kaveney, M. Nocente, E. P. Cippo, M. Rebai, B. Syme, M. Tardocchi, and JET-EFDA Contributors, Rev. Sci. Instrum. **85**, 043506 (2014).

[28]A. Pietropaolo, C. Andreani, M. Rebai, L. Giacomelli, G. Gorini, E. Perelli Cippo, M. Tardocchi, A. Fazzi, G. Verona Rinati, and C. Verona, Europhys. Lett. **92**, 68003 (2010).

[29]M. Rebai, D. Rigamonti, S. Cancelli, G. Croci, G. Gorini, E. Perelli Cippo, O. Putignano, M. Tardocchi, C. Altana, M. Angelone *et al.*, Nucl Instrum. Methods Phys. Res., Sect. A **946**, 162637 (2019).